EXPERIMENTAL STUDY OF SMECTITE INTERACTION WITH METAL Fe AT LOW TEMPERATURE: 1. SMECTITE DESTABILIZATION — Source link ↗

Sébastien Lantenois, Bruno Lanson, Fabrice Muller, A. Bauer ...+2 more authors

Institutions: University of Orléans, Centre national de la recherche scientifique, French Alternative Energies and Atomic Energy Commission

Related papers:

- The effect of iron on montmorillonite stability. (II) Experimental investigation

- Experimental synthesis of chlorite from smectite at 300ºC in the presence of metallic Fe

- Experimental study of the transformation of smectite at 80 and 300°C in the presence of Fe oxides

- Modelling iron–clay interactions in deep geological disposal conditions

- Experimental studies of the interactions between anaerobically corroding iron and bentonite

Experimental study of smectite interaction with metal iron at low temperature: 1. Smectite destabilization.

Sébastien Lantenois, Bruno Lanson, Fabrice Muller, Andreas Bauer, Michel Jullien, Alain Plançon

HAL Id: hal-00022201

https://hal-insu.archives-ouvertes.fr/hal-00022201

Submitted on 4 Apr 2006

Experimental study of smectite interaction with metal iron at low temperature: 1. Smectite destabilization.

Sébastien Lantenois[1] *, Bruno Lanson[2], Fabrice Muller[1], Andreas Bauer[3], Michel Jullien[4], Alain Plançon[1]

(1) Institut des Sciences de la Terre d'Orléans (ISTO), CNRS – Université d'Orléans, 1A rue de la Férollerie, 45071 Orléans Cedex 2, France.

(2) Environmental Geochemistry Group, LGIT, Maison des GéoSciences, Université J. Fourier – CNRS, BP 53, 38041 Grenoble Cedex 9, France.

(3) Institut für Nukleare Entsorgung, Forschungzentrum Karlsruhe, P.O. Box 3640, 76021 Karlsruhe Germany.

(4) Commissariat à l'Energie Atomique (CEA), Centre d'Etude de Cadarache DEN/DTN/SMTM/Laboratoire de Modélisation des Transferts dans l'Environnement , Bat 307, 13108 Saint Paul Lez Durance Cedex, France.

* Author to whom correspondence should be addressed.
e-mail: sebastien.lantenois@univ-orleans.fr

KEYWORDS: nuclear waste disposal, engineered barrier, clay barrier, iron-clay interactions, iron corrosion, clay stability, X-ray diffraction, smectite.

22   ABSTRACT

23

24   Interaction between metal iron and a variety of natural and synthetic smectites samples with

25   contrasting crystal chemistry was studied by scanning electron microscopy and X-ray

26   diffraction (XRD) from experiments conducted at 80°C. These experiments demonstrate an

27   important reactivity contrast as a function of smectite crystal chemistry. An XRD

28   quantification method involving the use of an internal standard allowed quantification of the

29   relative proportion of smectite destabilized as a function of initial pH conditions as well as of

30   smectite structural parameters. In mildly acidic to neutral pH conditions, a significant

31   proportion of metal iron is corroded to form magnetite without smectite destabilization. Under

32   basic pH conditions, smectite and metal iron are partly destabilized to form magnetite and

33   newly-formed 1:1 phyllosilicate phases (odinite and crondstedtite). Systematic destabilization

34   of both metal iron and smectite is observed for dioctahedral smectites while trioctahedral

35   smectites are essentially unaffected under similar experimental conditions. Smectite reactivity

36   is enhanced with increasing Fe^{3+} content and with the presence of Na^+ cations in smectite

37   interlayers. A conceptual model for smectite destabilization is proposed. This model involves

38   first the release of protons from smectite structure, $MeFe^{3+}OH$ groups being deprotonated

39   preferentially and metal iron acting as proton acceptor. Corrosion of metal iron results from

40   its interaction with these protons. Fe^{2+} cations resulting from this corrosion process sorb on

41   the edges of smectite particles and lead to induce the reduction of structural Fe^{3+} and migrate

42   into smectite interlayers to compensate for the increased layer charge deficit. Interlayer Fe^{2+}

43   cations subsequently migrate to the octahedral sheet of smectite because of the extremely

44   large layer charge deficit. At low temperature, this migration is favored by the reaction time

45   and by the absence of protons within the di-trigonal cavity. Smectite destabilization results

46   from the inability of the tetrahedral sheets to accommodate the larger dimensions of the newly

47   formed trioctahedral domains resulting from the migration of Fe^{2+} cations.

INTRODUCTION

49

50   In some of the "multi-barriers" concepts envisaged for the storage of high- and

51   intermediate-level and/or long-lived nuclear waste, metallic containers filled with vitrified

52   nuclear waste are placed in a confinement barrier itself surrounded by a geological barrier.

53   The reactive components of the engineered and geological barriers are clays (mainly

54   smectites) while metallic containers could be made up of iron. To predict the long-term

55   properties of these clay barriers, it is thus essential to study the interactions between clay

56   minerals, and more especially smectite, and metal iron as the corrosion of the metallic canister

57   could induce in turn the destabilization of the clay minerals.

58   Studies of these iron-clay interactions have shown indeed the partial but systematic

59   destabilization of the initial clay material and the subsequent crystallization of reaction

60   products (Habert, 2000; Perronnet, 2001, 2004; Kohler, 2001; Lantenois, 2003; Guillaume *et*

61   *al.,* 2003). The nature of these reaction products depends on experimental conditions such as

62   temperature and, to a minor extent, the nature of the initial clay material. When smectite is

63   used, iron-rich chlorite-like species are synthesized at high temperature (300°C - Guillaume *et*

64   *al.,* 2003) whereas iron-rich serpentine-like species are obtained for temperatures more

65   realistic in the context of nuclear waste disposal (80°C - Habert, 2000; Perronnet, 2001, 2004;

66   Lantenois, 2003). Newly formed 1:1 phyllosilicates with low iron content were also identified

67   by Kohler (2001) after reaction between iron metal and kaolinite/smectite mixtures at 80°C.

68   As reaction pathways appear to vary significantly as a function of temperature

69   (Guillaume *et al.,* 2003; Lantenois, 2003), it is especially important to work at temperatures

70   similar to those expected during storage lifetimes, thus generally excluding medium-to-high

71   temperature experiments (>200°C). Experimental conditions have been chosen to mimic those

72   of the repository, and experiments were thus performed in an anoxic and reducing

73 environment. The clay materials used for this study were essentially natural smectites which

74 have swelling and self-healing abilities and cation retention properties suitable for engineered

75 barriers. To promote the reactivity of clays so that significant reaction progress could be

76 obtained on a laboratory-compatible timescale, the water/solid ratio was significantly

77 increased.

78 A method has been developed to quantify the amount of smectite destabilized as a

79 result of its interaction with metal iron. The aim of the present study was to determine the role

80 of the nature of clay minerals on the contrasting reactivity observed during their hydrothermal

81 reaction with iron metal by using a variety of starting materials. Specifically, the structural

82 characteristics responsible for these differences were sought, together with the mechanism of

83 clay destabilization. The companion paper (Lantenois *et al.*, 2005) will describe the crystal-

84 chemistry of newly-formed phases.

85

86   MATERIALS AND METHODS

87

88 *Materials*

89

90 A variety of natural and synthetic smectite samples with contrasting crystal chemistry

91 were used in the present study. These samples were selected to include both di- and

92 trioctahedral varieties, smectite with octahedral or tetrahedral substitutions, and to cover a

93 wide range of chemical composition, focusing on the iron content. Chemical compositions of

94 selected samples are reported in Table 1. Untreated bulk samples were ground in an agate

95 mortar to increase their reactivity, but samples were neither size-fractionated nor purified.

96 Synthetic clays were crystallized from gels under hydrothermal conditions. Gels were

97 prepared following a method adapted from Hamilton and Henderson (1968) using tetraethyl

98   orthosilicate (TEOS), $Mg(NO_3)_2.6H_2O$, $Al(NO_3)_3.9H_2O$, $Fe(NO_3)_3.9H_2O$, HNO_3, Na_2CO_3,

99   NH_4OH and ethanol. All reagents had a 99% minimum grade. After dissolution of Al- and

100   Mg-nitrates and of Na_2CO_3 in nitric acid, TEOS and ethanol were added. A precipitate was

101   obtained by neutralizing the resulting solution at pH ~ 6 with addition of NH_4OH. This

102   precipitate was dried at 80°C for 24 hours, ground in an agate mortar and heated to 400°C to

103   remove nitrates and carbonates and to obtain a gel composed essentially of Al, Mg, Si and Na

104   oxides. SapFe08 saponite was synthesized from such gels in a cold-sealed pressure vessel.

105   Gel and deionized water were introduced in a 2:1 weight ratio in a silver tube itself placed in

106   the vessel heated at 400°C for one month at an estimated pressure of 100 MPa (Suquet *et al.*,

107   1977). The SbS-1 beidellite was synthesized in an internally heated pressure vessel. 600 mg

108   of gel were mixed to 1.3 g of a NaOH solution (0.2N) in a gold tube. The tube was then

109   sealed and heated to 350°C under 22 MPa for 10 days (Klprogge *et al.*, 1999). After cooling

110   of the vessels, the solid products were extracted from the reaction tubes, dried at 80°C

111   overnight, and ground before structural and chemical characterization using X-ray diffraction

112   (XRD) and energy dispersive X-ray fluorescence spectroscopy (EDS) on a transmission

113   electron microscope (TEM).

114   To better assess the role of the interlayer composition on the reaction rate K-, Na-, and

115   Ca-saturated specimens were prepared for samples SWy-2, Garfield, and SAz-1. The cation

116   exchange procedure was performed at room temperature by immersing the ground clay

117   sample in 1M KCl, NaCl or $CaCl_2$ aqueous solutions. After 12 hours of contact, the solid was

118   extracted by centrifugation. The saturation procedure was repeated four times. The excess

119   chloride was then removed by washing the sample five times with distilled water (K- and Ca-

120   saturated samples). Na-saturated samples were washed once in ethanol, and then dialysed in

121   deionized water for one week.

122

Experimental

124

125   For the iron-clay interactions, 0.6 g of the clay powder were mixed with 0.6 g of metal

126   iron powder (10 µm maximum size, Merck[®] product for analysis) to maximize the contact

127   surface between iron and clay particles. The large amount of metal iron was intended also to

128   promote reducing conditions during the experiments. 30 mL of water were added to this

129   initial mixture. Deionized water (with a resistivity >18MΩ cm^{-1}) was used to allow studying

130   the final solution composition. Samples were prepared in a MBraun[®] glove box equipped with

131   copper catalysts to eliminate O_2, and a MBraun[®] O_2 control system. Partial pressure of O_2 was

132   lower than 1 ppm during sample preparation. Deionized water was degassed with Argon for

133   one hour prior to its introduction in the glove box and all products were allowed to stay in the

134   glove box for 24 hours to equilibrate with the glove box atmosphere. Starting products were

135   then placed in 40 mL Nalgene[®] reactors. Because these reactors are oxygen porous, a "double

136   enclosure system" was used where the Nalgene[®] reactors were inserted into larger Teflon[®]

137   reactors which contain metal iron powder, $FeSO_4$ and water. Any oxygen entering the Teflon

138   reactors was thus eliminated according to reactions (1) and (2) with ferrous and metal iron,

139   respectively (Aogaki, 1999).

$$2Fe^{2+}+ 1/2O_2 + 3H_2O \rightarrow 4H^+ + 2FeOOH \qquad (1)$$

$$2Fe° + 3/2O_2 + 3H_2O \rightarrow 2Fe(OH)_3 \qquad (2)$$
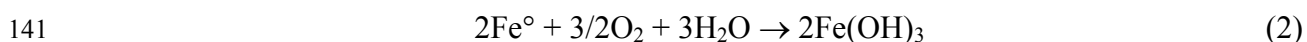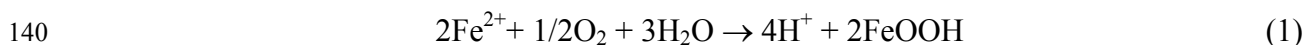
142   The two reactors were tightly closed within the glove box and subsequently heated at

143   80°C for 45 days outside of the glove box. Additional experiments were also performed for 5,

144   15, 30, 60, 90 and 120 days on selected samples (Garfield, SbId, SWy-2 and SapCa-2). At the

145   end of the reactions, reactors were cooled down to room temperature and opened in air, the

146   solution pH being measured immediately. The solution was subsequently filtered (0.45 µm)

147   and acidified for chemical analysis, whereas the solid fraction was dried at 80°C overnight

148   and ground.

149   Filtered solutions were analyzed for major and trace elements (Si, Al, Fe, Mg, Ti, Na,

150   Ca and K) with an ICP-AES Jobin-Yvon ULTIMA spectrometer. Scanning electron

151   microscopy (SEM) was performed using a JEOL 6400 microscope. Samples were covered

152   with a Au film before observation to avoid charge build up. TEM was performed using a

153   JEOL 2000 FX microscope operated at 200 kV. Samples were prepared as a suspension in

154   deionized water, a drop of this suspension being dried on copper grids covered with a carbon

155   film.

156   Powder XRD patterns were recorded in transmission geometry using CoKα radiation

157   (35 mA, 35 kV) to avoid iron fluorescence. The use of an INEL CPS 120 curved position

158   sensitive detector allowed recording simultaneously the diffracted intensity over a 4-50°2θ

159   range with a step size of 0.03°. The non-linearity of the detector was corrected (Roux and

160   Wolfinger, 1996). A 0.5 mm diameter Lindemann glass tube was used to hold the sample

161   powder.

162   Infrared (IR) spectra were recorded over the 650–4000 cm^{-1} range with a 2 cm^{-1}

163   resolution using a Nicolet Magna-IR Fourier transform spectrometer equipped with a Globar

164   SiC source and a DTGS detector. The spectrometer was purged with dry air prior to data

165   collection to remove most of atmospheric H_2O. The sample was finely ground in an agate

166   mortar, and 0.5 mg of the resulting powder was mixed to 150 mg of KBr previously dried at

167   120°C for 24 hours. The mixture was homogenized and pressed in an evacuable die to

168   prepare a 12 mm diameter pellet. Decomposition of the IR spectra in the OH bending region

169   (700 – 900 cm^{-1}) was performed with Peak-Fit (v4.05).

170   The cation exchange capacity (CEC) was measured using the copper complex method

171   (Gaboriau, 1991). 600 mg of sample were suspended for 12 hours in 25 mL of a 0.02 N

172 ethylene di-amine copper complex (Cu(EDA)$_2$Cl$_2$) solution. After centrifugation, the Cu

173 concentration in solution was measured using a 905-GBC atomic absorption

174 spectrophotometer from GBC Scientific Equipment.

175

176 *Quantification of the relative proportion of smectite destabilized after reaction*

177

178 To estimate reaction progress, the amount of residual smectite was quantified by XRD

179 using the internal standard technique adapted to clays by Hillier (2000). As recommended by

180 this author, each sample was mixed with 10% of a corundum internal standard (particle size

181 < 50μm), dry ground in an agate mortar for 10 minutes and then introduced in the Lindeman

182 glass tube. The use of a glass tube in transmission geometry allows optimizing sample

183 disorientation. Segregation due to particle size and/or particle density was minimized by

184 careful grinding and mixing. Absorption corrections have not been considered because

185 absorption, which is closely related to sample chemical composition, is similar before and

186 after reaction.

187 The (001) reflection of smectite was not selected for quantification, because its

188 intensity strongly depends on smectite hydration state and thus on the chemical composition

189 of smectite interlayers, which can be modified during the reaction. The amount of residual

190 smectites was rather quantified by measuring the integrated intensity of the (02,11) band

191 (between 22.0° and 27.0°2θ CoKα - Figure 1) before and after reaction, these intensities

192 being normalized to the (012) reflection of corundum (29.8°2θ CoKα - Figure 1).

193 Background was assumed to be linear between 22.0 and 27.0°2θ and subtracted. If quartz

194 impurities were present, the (100) reflection of quartz (~24.3°2θ CoKα) was fitted, and its

195 integrated intensity subtracted from the total integrated intensity. To assess the validity of

196 XRD results, the relative proportion of reacted smectite was also quantified from CEC

197 measurements performed before and after reaction, the observed CEC decrease being directly

198 linked to the amount of destabilized smectite. This assumption was made possible by the non-

199 swelling character of the reaction products (Lantenois, 2003; Lantenois *et al.*, 2005).

200   The amount of residual smectite was also quantified using IR spectroscopy. Over the

201 OH bending frequency range, three bands at 912-920 cm^{-1}, 874-886 cm^{-1}, and 840-850 cm^{-1}

202 correspond to the Al-Al-OH, Al-Fe-OH and Al-Mg-OH vibrations of smectites, respectively

203 (Farmer, 1974; Goodman *et al.*, 1976; Russell and Fraser, 1994; Vantelon *et al.*, 2001). The

204 position reported in the literature for the Fe-Fe-OH band scatters from 820-795 cm^{-1}

205 (Goodman *et al.*, 1976; Cuadros and Altaner, 1998) and overlaps with the Si-O vibrations of

206 quartz at 780 and 800 cm^{-1} (Madejova and Komadel, 2001). To avoid using this problematic

207 band, reaction progress was quantified using IR spectroscopy for Fe-poor smectites only. The

208 quantification method itself requires subtracting a baseline which corresponds to Si-O

209 vibrations in phyllosilicates (Figure 2a − Vantelon *et al.*, 2001). A cubic spline baseline,

210 similar for all samples, was adjusted on both sides of the region of interest (817-822 cm^{-1} and

211 940-945 cm^{-1}, respectively). The 822-945 cm^{-1} range of the baseline-corrected spectra was

212 then fitted with three Gaussian-shaped curves (Figures 2b) corresponding to Al-Al-OH, Al-

213 Fe-OH and Al-Mg-OH vibration modes. Relative proportion of unaltered smectite was

214 estimated from the ratio between the total surface areas determined for these three

215 contributions before and after reaction.

216

RESULTS

218

219 *Qualitative evaluation of the reaction progress*

220

221   Long-term experiments show that the reaction progress reaches a plateau after about

222 30 days (see below). Except when specifically notified, reactions described in the following

223 section were thus performed for 45 days, without constraining the solution pH. The observed

224 reaction depends on the nature of the initial smectite sample. In particular di- and tri-

225 octahedral smectites exhibit contrasting reactivities and will be described separately.

226 *Dioctahedral smectites*. Although reaction progress varies considerably as a function of the

227 initial smectite sample, a similar effect was observed for all dioctahedral smectites. After 45

228 days, solution pH was not significantly modified, whereas the chemical composition of the

229 solutions was altered (Table 2). In particular, the concentration in solution of alkali and alkali-

230 earth cations which were initially present in smectite interlayers (Na^+, Ca^{2+}, and K^+) was

231 significantly increased after reaction (Table 2) together with that of silicon. For smectite

232 samples reacted without metal iron, Si was not detected in solution, and the concentration in

233 solution of alkali and alkali-earth cations after reaction was lower than in similar experiments

234 performed in presence of metal iron (Table 2). In all reacted samples residual metal iron was

235 systematically present together with newly-formed phases (magnetite and 7 Å phyllosilicates

236 – Figure 1a-e). However, iron particles observed in all reacted samples appear corroded as

237 compared to their initial state (Figure 3a,b). In addition, clay particles with a distinct

238 morphology were observed in all reacted samples (Figure 3c). These particles most likely

239 correspond to the newly-formed phyllosilicate phase. Unreacted clay particles were also

240 observed for both montmorillonite and beidellite samples (Figures 3d,e). Accordingly,

241 residual smectite was identified for montmorillonite and beidellite samples from its (02,11)

band at ~23°2θ CoKα (Figure 1a-d). The intensity of this characteristic band was much

reduced after reaction for Garfield nontronite sample (Figure 1e), in agreement with the

absence of unreacted clay particles in the reacted Garfield sample (Figure 3f).

Trioctahedral smectites. For saponite samples, solution pH and composition are not

significantly modified after 45 days of iron-clay interactions (Table 2). Accordingly, XRD

patterns recorded on both unreacted and reacted samples are alike (Figure 1f). In particular,

the (02,11) band (~23°2θ CoKα) is similar in both samples, an even the (001) reflection

(~7°2θ CoKα) is practically unaffected. In addition, no extra reflection was visible after

reaction. SEM observations support this lack of reactivity as both iron (not shown) and clay

particles (Figures 3g,h) appear unaltered after 45 days.

Quantification of the extent of smectite destabilization

A quantitative estimate of the relative proportion of smectite destabilized after

reaction was obtained from XRD results using the internal standard method (Hillier, 2000).

Results of this quantification are presented in Table 1. The absolute precision on the relative

proportion of smectite destabilized was estimated to be ±10%. This estimate corresponds to

the standard deviation of twelve measurements obtained for 45 day experiments performed

with sample SWy-2.

Using this quantitative XRD method it was possible to demonstrate the reactivity

contrast as a function of the nature of initial smectite samples. For the different smectites

presented in Figure 1, the relative proportion of destabilized smectite scatters indeed from 0-

95%. Trioctahedral smectites (SapCa-2 and SapFe08 samples) were essentially unaffected as

a result of their interactions with iron, while the dioctahedral smectites were systematically

destabilized. Montmorillonite (20 and 50% of destabilized smectite for SAz-1 sample and

267 SWy-2 samples, respectively) and beidellites (40, 60 and 70% of destabilized smectite for

268 CP4, SbId, and Drayton samples, respectively) were less destabilized than ferruginous

269 smectites or nontronites (90 and 95% of destabilized smectite for SWa-1 and Garfield

270 samples, respectively).

271   These quantification results were positively correlated to the estimates made using

272 CEC measurements (Figure 4a). The precision of the CEC determination (±10%), which

273 corresponds to the standard deviation of six measurements obtained for 45 day experiments

274 performed with sample SWy-2, is similar to that of the XRD method. A good correlation was

275 also obtained with the IR quantification results except for the Drayton sample (Figure 4b)

276 which contains a significant proportion of ferric iron (0.47 per $O_{10}(OH)_2$ – Table 1). Precision

277 was estimated from the standard deviation of six measurements obtained for 45 day

278 experiments performed with sample SWy-2. IR measurements of reaction progress were

279 found to be less precise (±15%) than those using XRD and CEC methods mostly as a result of

280 the uncertainty on the baseline determination. In addition, note that IR results obtained on raw

281 materials may be correlated with XRD data only in the absence of kaolinite which exhibits a

282 band at 911 cm^{-1} which may interfere with the Al-Al-OH, Al-Fe-OH and Al-Mg-OH vibration

283 modes.

284   For the three quantification methods, the possible influence of the newly-formed clay

285 phases was neglected. This approximation was justified by the nature (crondstedtite, odinite)

286 of the newly-formed phases (Lantenois, 2003; Lantenois *et al.*, 2005). These 1:1

287 phyllosilicates were indeed non-swelling species thus exhibiting an extremely low CEC. In

288 addition, these phases include a large amount of structural iron. As a result, the (02,11) band

289 of these iron-rich 1:1 phyllosilicates was significantly shifted towards lower angles (at

290 ~4.7 Å) as compared to the (02,11) band of initial smectite samples (at 4.45-4.56 Å for the

291 whole compositional range). In addition the intensity of the (02,11) band of these iron-rich 1:1

292 phyllosilicates was found to be extremely low, thus not affecting significantly the XRD

293 measurements (Lantenois, 2003; Lantenois *et al.*, 2005). The OH bending bands observed for

294 these iron-rich 1:1 phyllosilicates were also shifted towards lower frequencies (750-800 cm^{-1}

295 – Lantenois, 2003; Lantenois *et al.*, 2005) as compared to initial Al-rich smectites (820-

296 940 cm^{-1}).

297

298 *Kinetics of smectite destabilization*

299

300   XRD quantification of the relative proportion of smectite destabilized after reaction

301 also allowed deriving the kinetics of this destabilization reaction. For example, XRD patterns

302 obtained for samples SbId reacted for 0, 5, 15, 30 and 45 days are presented in Figure 5.

303 These experimental patterns are normalized to the (012) reflection of corundum so that the

304 relative intensity of the (02,11) band can be compared for all samples. The relative proportion

305 of smectite destabilized was estimated from the intensity decrease of this (02,11) band as a

306 function of reaction time (0-120 days). Results are plotted in Figure 6 for four samples (SbId,

307 Garfield, SWy-2 and SapCa-2). As described qualitatively, no reaction was observed for

308 sample SapCa-2. For dioctahedral smectites, the relative proportion of destabilized smectite

309 increases with time to reach a steady-state plateau after 30-45 days. The amount of

310 destabilized smectite obtained after 45 days can be considered as the final one for all

311 smectites. As was qualitatively observed the extent of smectite destabilization varies

312 significantly as a function of the initial samples (50%, 60% and 95% of destabilized smectite

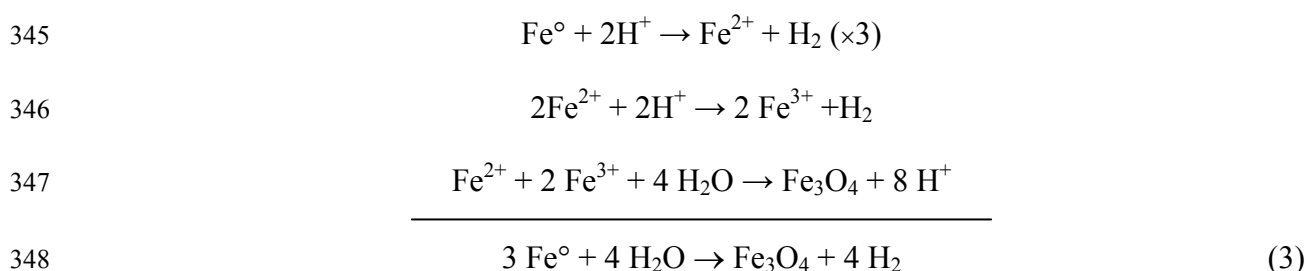313 for the SWy-2, SbId and Garfield samples, respectively)

314

Quantification by XRD of the relative proportion of destabilized smectite allowed demonstrating that reaction progress strongly depends on the nature of the initial smectite sample, and that reaction kinetics cannot account for the reactivity contrast between different smectite samples. In the following discussion, the origin of these contrasting reactivities will be sought, and the influence of some structural characteristics of smectites will be discussed to hypothesize reaction mechanisms for the destabilization of smectite.

Influence of pH on smectite destabilization

The initial solution pH, which is obtained by equilibrating the different smectite samples in water, depends on the nature of the smectite, and varies from 7.5-10.5 (SbId-1 and SWy-2, respectively – Table 2). To assess the impact of this parameter on reaction progress, the relative proportion of destabilized smectite was determined as a function of the initial pH for sample SWy-2. Initial pH was adjusted by adding HCl or NaOH to the initial mixture. Relative proportion of destabilized smectite is reported in Table 3. When initial pH is basic (8-12 pH range), the nature of the reaction products and the reaction progress are independent on pH (Table 3). Conversely, reaction is dramatically different when initial pH is mildly acidic to neutral. In such case, a large proportion of metal iron is dissolved, whereas iron oxides, identified as magnetite using XRD (data not shown), precipitate extensively. In addition, smectite appears unaffected (Table 3). A similar reaction, with the precipitation of magnetite and the stability of smectite, was observed for SapCa-2 and Garfield samples when initial pH was mildly acidic to neutral (Table 3).

339   Under mildly acidic to neutral pH conditions such as those of the present study

340   (pH = 6), smectite remains unaltered in presence of metal iron whatever its nature. However,

341   smectite plays a catalytic role as in the same experimental conditions (45 days, 80°C , initial

342   pH = 6) metal iron is not destabilized in the absence of smectite whereas in presence of

343   smectite metal iron is oxidized, most likely from its interaction with solution protons, to form

344   magnetite according to the following reaction:

345
$$Fe° + 2H^+ \rightarrow Fe^{2+} + H_2 \ (\times 3)$$

346
$$2Fe^{2+} + 2H^+ \rightarrow 2\ Fe^{3+} + H_2$$

347
$$\underline{Fe^{2+} + 2\ Fe^{3+} + 4\ H_2O \rightarrow Fe_3O_4 + 8\ H^+}$$

348
$$3\ Fe° + 4\ H_2O \rightarrow Fe_3O_4 + 4\ H_2 \qquad\qquad (3)$$

349   In our experiments, the production of gaseous H_2 during the reaction was not

350   observed as Nalgene$^{®}$ reactors were H_2 porous.

351   Under more basic pH conditions (pH > 7 obtained from the addition of NaOH if

352   necessary), the reaction is dramatically different as dioctahedral smectites are involved in the

353   reaction. Dioctahedral smectites are then destabilized to form new clay phases according to

354   the following reaction:

355   Metal iron + smectite $\rightarrow$ 1:1 iron-rich phyllosilicate + iron oxides   (4)
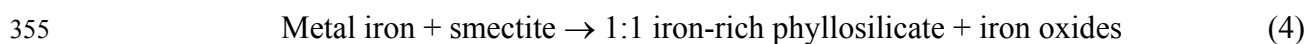
356   Under these basic pH conditions, destabilization of dioctahedral smectite is

357   systematic but the amount of destabilized smectite varies significantly from one sample to the

358   other most likely as a function of the initial smectite crystal chemistry. Note that except for K-

359   saturated smectites the equilibration pH of smectite with water is basic. The pH is essentially

360   unaffected by iron-clay interactions.

361

Influence of smectite crystal chemistry on smectite destabilization

363

364 *Influence of the di- or tri-octahedral character.* Although initial pH values are alike, and

365 basic, for both di- and tri-octahedral smectites, the reactivity of trioctahedral smectites is

366 strikingly different from that of dioctahedral ones. Dioctahedral smectites are indeed

367 systematically destabilized as the result of their interaction with metal iron whereas

368 trioctahedral smectites remain unaffected under similar experimental conditions (Figures 1,

369 6). This lack of reactivity is independent on the iron content of trioctahedral smectites and on

370 the nature of the interlayer cation.

371 *Influence of structural Fe^{3+}.* As can be seen in Figure 6 and in Table 1, nontronite and

372 ferruginous smectites are thoroughly destabilized as the result of their interaction with metal

373 iron. In both cases, Fe^{3+} is the predominant cation in the octahedral sheet of these 2:1

374 expandable phyllosilicates which exhibit mostly tetrahedral substitutions (Table 1). By

375 contrast, the extent of the destabilization is much reduced for smectites that are not iron-rich,

376 whatever the origin of the layer charge deficit. However, this decrease of reactivity is less

377 important for beidellites (tetrahedral layer charge) than for montmorillonites (octahedral layer

378 charge) for a given Fe^{3+} content. To illustrate further the influence of the amount of structural

379 iron on smectite destabilization, XRD patterns of reacted and unreacted samples are compared

380 in Figures 1 and 7 for dioctahedral smectites with predominant tetrahedral charges

381 (beidellites). Their octahedral Fe^{3+} content which ranges from 0.0-1.9 per $O_{10}(OH)_2$. Relative

382 proportions of destabilized smectites are reported as a function of the Fe^{3+} content in Figure 8.

383 No reaction is observed when no structural Fe^{3+} is present in dioctahedral smectites, and

384 smectite is not destabilized (Figures 7a, 8). The presence of structural Fe^{3+} is thus an essential

385 condition for the destabilization of dioctahedral smectites when in contact with metal iron.

386 The minimum amount of structural Fe^{3+} necessary to induce this destabilization is extremely
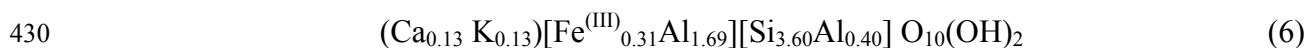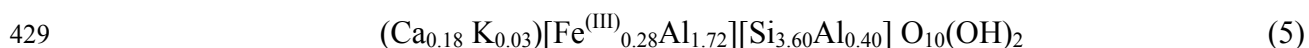
387　low as 60% of samples SbId is destabilized after 45 days of reaction with metal iron, in spite

388　of its limited Fe^{3+} content (0.1 atom per $O_{10}(OH)_2$). In addition to this essential triggering

389　role, the reactivity of dioctahedral smectite is clearly enhanced by an increased content of

390　octahedral Fe^{3+} (Figure 8). However, this parameter is not the only structural parameter

391　influencing smectite reactivity as, for example, the relative proportion of destabilized smectite

392　is much higher for sample SbId than for sample CP4, in spite of the higher Fe^{3+} content in the

393　latter sample (Figures 1c,d, 8 – Table 1).

394　*Influence of the interlayer cation composition*. The cation composition of smectite interlayers

395　appears as an additional parameter influencing the reactivity of dioctahedral smectites. All

396　samples used in the experiments reported to this point were unprocessed, and Ca^{2+} was

397　usually predominant in their interlayer spaces (Table 1). However, K^+ was also present in CP4

398　and SbId, whereas Na^+ was present in several samples (SbId, SWy-2, SAz-1), and Mg^{2+} in

399　Drayton sample. To assess the influence of the interlayer cation composition on smectite

400　reactivity, three smectite samples (SWy-2, SAz-1 and Garfield) were reacted with metal iron

401　following their saturation with Na^+, Ca^{2+}, and K^+. XRD patterns of reacted SWy-2 samples

402　are presented in Figure 9, whereas the relative proportions of smectite destabilized after 45

403　days of reaction with metal iron are reported in Table 4. If Ca-saturated smectites are used as

404　a reference, smectite destabilization is enhanced for Na-saturated smectites whereas it is

405　decreased for K-saturated samples.

406　The reactivity contrast observed as a function of the interlayer cation composition is most

407　likely related to the hydration of smectite which varies as a function of the interlayer cation

408　(Norrish, 1954; Pons *et al.*, 1981). The $d_{(001)}$ basal spacing of K^+-saturated smectites varies

409　indeed from 12.5-15.5 Å in aqueous solution (Mamy, 1968; Besson and Tchoubar, 1980),

410　whereas that of Ca^{2+}-saturated smectites is 18.6-19.2 Å (Suquet, 1978). The $d_{(001)}$ basal

411　spacing of Na^+-saturated smectites is not limited (osmotic swelling – Suquet *et al.*, 1981). No

412 significant collapse of smectite interlayers is expected as the ionic strength of the solutions,

413 and more specifically the concentration of alkali and alkali-earth cations, remains low after

414 reaction (Table 2). The enhanced reactivity observed for the most hydrated samples ($Na^+ >$

415 $Ca^{2+} > K^+$) indicates that the ability of solution cations to access smectite interlayers is a key

416 parameter to smectite destabilization.

417   Accordingly, the interlayer cation composition of samples CP4 ad SbId is likely

418 responsible for their contrasting reactivity which does not seem to be consistent with their

419 respective Fe^{3+} contents (Figure 8, Table 1). Specifically, the presence of Na^+ in the

420 interlayers of sample SbId most likely enhances its reactivity as compared to sample CP4 in

421 spite of the higher iron content in the latter sample. The influence of the cation interlayer

422 composition may also account for the different reactivity exhibited by populations of particles

423 observed in sample CP4. Using TEM-EDX, two populations of particles were indeed

424 differentiated from their morphology, as "rolled" and "flat" particles were identified in this

425 sample (Figure 10). The chemical analysis of these two types of particles revealed that

426 although the composition of the 2:1 layers was identical in both cases, the two populations

427 differed by their interlayer cation composition as the following structural formulae were

428 derived for "rolled" and "flat" particles, respectively (average values from twelve analyses):

429 $$(Ca_{0.18} K_{0.03})[Fe^{(III)}_{0.28}Al_{1.72}][Si_{3.60}Al_{0.40}] O_{10}(OH)_2 \qquad (5)$$

430 $$(Ca_{0.13} K_{0.13})[Fe^{(III)}_{0.31}Al_{1.69}][Si_{3.60}Al_{0.40}] O_{10}(OH)_2 \qquad (6)$$

431   After reaction with metal iron, no remnant "rolled" particles were observed and only

432 "flat" particles persisted. This is likely due to the increased proportion of K^+ in the interlayer

433 of the latter particles which reduces their reactivity. Note that because long-term experiments

434 were not performed on homoionic samples, it is not clear if the relative proportion of smectite

435 ultimately destabilized varies from one cation to the other, or if the nature of the interlayer

436 cation essentially influences the destabilization rate.

437

Towards a possible model for smectite destabilization

439

Experimental constrains. From the above observations, several structural features appear as essential to the destabilization of smectite when in contact with metal iron. First, the smectite should be dioctahedral and should contain octahedral Fe^{3+}. In addition, the accessibility of its interlayer space is a key parameter for the apparent reactivity of the dioctahedral smectite. Finally, when comparing experiments run at different pH values, structural protons of the smectite are likely involved in the oxidation of metal iron under neutral-to-alkaline conditions. In mildly acidic to neutral conditions, solution protons are abundant enough so that smectite is used essentially as a catalyst but is not directly involved in the corrosion of iron following Reaction (3). Under high pH conditions, protons are essentially present as OH groups in smectite, as both smectite interlayer and edge sites are essentially deprotonated under such pH conditions.

Deprotonation of these hydroxyl groups may occur under a variety of physico-chemical conditions for dioctahedral smectites (Russel, 1979; Jaymes and Bigham, 1987; Heller-Kallai and Rozenson, 1981; Heller-Kallai, 2001 – Figure 11a). In particular, the presence of inorganic proton acceptors, usually alkali halides or alkali hydroxides, has been reported to induce such a deprotonation reaction (Heller-Kallai, 1975a, 1975b, 2001; Russel, 1979; Heller-Kallai and Rozenson, 1981; Heller-Kallai and Mosser, 1995). In our case, metal iron is likely the proton acceptor triggering smectite deprotonation. Metal iron is oxidized in turn as the result of its interaction with protons (Figure 11b) according to Reaction (3). The high affinity of metal iron for smectite and their resulting interactions have for example been recognized as causing the oxidation of steel pipes when using clay-containing drilling fluids (Tomoe *et al.*, 1999; Cosultchi *et al.*, 2003). According to this model, both the oxidation of

462 metal iron and the deprotonation of smectite are strongly favored by the accessibility of metal

463 iron to smectite interlayer. With this respect the osmotic swelling commonly observed for Na-

464 saturated smectites significantly enhances the accessibility of metal iron particles to smectite

465 interlayers, thus favoring the deprotonation reaction. In turn, deprotonation increases

466 considerably the layer charge deficit in smectite octahedral sheet and thus enhances their

467 reactivity.

468   Deprotonation thus appears as the driving force for the oxidation of metal ion, and for

469 the initiation of smectite destabilization. Accordingly, the presence of Fe^{3+} in the octahedral

470 sheet of smectite appears as an essential parameter for these two reactions as $MeFe^{3+}OH$

471 groups are known to deprotonate preferentially in dioctahedral smectites (Heller-Kallai,

472 1975a, 2001; Russel, 1979; Jaymes and Bigham, 1987). It is not clear however if

473 deprotonation of Fe^{3+}-free dioctahedral smectites is not occurring, or is extremely limited, or

474 if deprotonation is not the limiting step for the destabilization of Fe^{3+}-free dioctahedral

475 smectites. However, although Heller-Kallai (1975a) showed that deprotonation occurs even in

476 Fe^{3+}-free dioctahedral smectite, we have not observed iron corrosion resulting from this

477 process in the SbS-1 experiments.

478 *Destabilization of smectite.* Following its initial deprotonation, destabilization of smectite is

479 probably favored by the presence of Fe^{2+} in solution as a result of the oxidation of metal iron.

480 Specifically, the high affinity of Fe^{2+} for smectite edge surface sites (Tournassat *et al.*, 2005 –

481 Figure 11c) is likely a key factor for the subsequent destabilization of smectite. Following

482 their sorption on these edge sites, Fe^{2+} cations are readily oxidized as shown by Tournassat *et*

483 *al.* (2005), the electron acceptors being octahedral Fe^{3+} from smectite structure (Figure 11c).

484 Note that following their oxidation, sorbed Fe cations may also accept electrons either from

485 solution Fe^{2+} cations or from iron metal to restore their +II valency (Figure 11d). As a result

486 of both its initial deprotonation and of the subsequent reduction of its structural Fe^{3+}, the

487 charge deficit in the octahedral sheet of smectite is dramatically increased and Fe^{2+} cations

488 likely migrate in its interlayers to compensate for the increased layer charge (Figure 11d). The

489 inceased concentration of Fe^{2+} in solution resulting from the oxidation of the metal iron also

490 favors a Fe^{2+}-for-Na^+ cation exchange. Such Fe^{2+}-for-Na^+ cation exchange has been shown to

491 occur in reducing environments cations (Kamei *et al.*, 1999).

492   The effective ionic radius of Fe^{2+} cations (0.78 Å – Shannon, 1976) is smaller than the

493 limit size approximated by Heller-Kallai (2001) at 0.85 Å allowing migration of the cations

494 into the silicate layer. It is thus likely that interlayer Fe^{2+} cations actually migrate either into

495 the di-trigonal cavities of smectite tetrahedral sheets or in smectite octahedral sheet (Figure

496 11e). This migration is similar to that of Li^+ cations (0.76 Å – Shannon, 1976) involved in the

497 Hofmann-Klemen test (Hofmann and Klemen, 1950; Greene-Kelly, 1955). The migration of

498 Li^+ from the interlayer to the di-trigonal cavity and further to the octahedral sheet of

499 montmorillonites has been extensively documented (Hofmann and Klemen, 1950; Greene-

500 Kelly, 1955 ; Glaeser and Fripiat, 1976; Madejova *et al.*, 1996, 2000a, 2000b, among others).

501 Heating to 300°C for 24 hours represent optimum experimental conditions for this migration.

502 Migration of other divalent cations with an effective ionic radius similar to that of Li^+ cations

503 has also been described. For example, Cu^{2+}, Ni^{2+} and Zn^{2+} cations (0.73, 0.69 and 0.74 Å,

504 respectively) migrate from montmorillonite interlayers to the di-trigonal cavity between 100-

505 300°C (Heller-Kallai and Mosser, 1995; Mosser *et al.*, 1997; Madejova *et al.*, 1999; Palkova

506 *et al.*, 2003) and to the octahedral sheet at higher temperature (Brindley and Ertem, 1971;

507 McBride and Mortland, 1974; Heller-Kallai and Mosser, 1995; Emmerich *et al.*, 1999).

508   These conditions are much more energetically favorable than those involved in our

509 experiments. However, partial migration of Li at least to the di-trigonal cavity has been

510 reported for Li-saturated montmorillonite heated to 105°C for 24 hours (Madejova *et al.*,

511 1996). In our experiments, three factors compensate for the low thermal energy available. The

512   first one is the extremely strong layer charge deficit which, according to the structural model

513   proposed for smectite destabilization occurring in our experiments, arises both from the

514   deprotonation of hydroxyl groups and from the reduction of structural Fe^{3+}. Note that the need

515   for an octahedral layer charge deficit is the fundamental basis for the migration of Li^+ cations

516   involved in the Hofmann-Klemen test (Hofmann and Klemen, 1950). Furthermore, the

517   positive influence of an increased layer charge deficit on the migration of divalent cations has

518   been reported by Heller-Kallai and Mosser (1995, e.g.). These authors observed indeed an

519   increased amount of Cu in samples that were deprotonated first. As described by Heller-Kallai

520   and Mosser (1995), the positive effect of the initial deprotonation is not restricted to the

521   increased layer charge deficit and the second factor favoring the migration of Fe^{2+} cations is

522   the absence of protons inside the di-trigonal cavity. As a consequence, there is no electrostatic

523   repulsion to the migration of Fe^{2+} cations into the octahedral sheet. Reaction time represents

524   the third factor compensating for the low thermal energy in our experiments. Our experiments

525   lasted indeed for 45 days whereas the common duration of experiments leading to the

526   formation of reduced-charge smectites is 24 hours. Initial migration of Fe^{2+} cations to the di-

527   trigonal cavity is likely favored by an increased undersaturation of the oxygen atoms present

528   at the surface of the 2:1 layers, that is by the existence of layer charge deficit in smectite

529   tetrahedral sheets. Such location of layer charge deficit favors indeed the initial partial

530   dehydration of interlayer Fe^{2+} cations, allowing for the formation of an inner-sphere complex

531   necessary for their migration, and thus accounts for the increased reactivity of beidellite

532   samples as compared to montmorillonite ones for a given iron content (see for example SAz-1

533   and SbId samples – Table 1). The formation of such inner-sphere complexes has been widely

534   documented in hydrated beidellites for monovalent interlayer cations, both from XRD (Ben

535   Brahim *et al.*, 1983a, 1983b, 1984), and infrared (Pelletier *et al.*, 2003) studies, and from

536   Monte-Carlo modeling (Chang *et al.*, 1995; Skipper *et al.*, 1995).

537   In our experiments, migration of Fe^{2+} cations in the octahedral sheet of smectite does

538   not induce a collapse of smectite interlayers as these new octahedral Fe^{2+} compensate

539   essentially for the layer charge deficit resulting from the deprotonation of hydroxyl groups

540   and from the reduction of structural Fe^{3+}, but not for the initial charge deficit of the 2:1 layers.

541   The presence of hydrated interlayer cations, part of which are Fe^{2+}, still compensates for this

542   initial charge deficit, and keeps the smectite interlayers expanded. The migration of Fe^{2+}

543   cations in the octahedral sheet of smectite is rather thought to be responsible for the

544   destabilization of smectites induced by their interaction with metal iron. Destabilization is

545   indeed thought to result from the presence of trioctahedral domains in the octahedral sheet of

546   reacted smectite (Figure 11e). The coexistence of both dioctahedral and trioctahedral domains

547   is widely reported in natural 1:1 phyllosilicates but is limited in 2:1 phyllosilicates (Bailey,

548   1980). The existence of 2:1 phyllosilicates with a mixed di- and tri-octahedral occupancy is

549   indeed essentially limited to mica species exhibiting a tetrahedral charge (muscovite-

550   zinnwaldite or muscovite-phlogopite series – Monier and Robert, 1986). In such species the

551   increased dimensions of the octahedral sheet in the **ab** plane is accommodated by the

552   reduction of the tetrahedral tilt angle. In smectites, and more especially in montmorillonites,

553   the amount of tetrahedral substitutions is limited and the tetrahedral tilt angle is thus

554   minimum. As a consequence, such 2:1 phyllosilicates are unable to accommodate the

555   presence of trioctahedral domains containing large cations and are thus destabilized by the

556   migration of Fe^{2+} cations in their octahedral sheet.

557   According to the conceptual model hypothesized for smectite destabilization, the lack

558   of reactivity of trioctahedral smectites results from three main factors. The first two are

559   related to the absence of Fe^{3+} cations in the octahedral sheet of these smectite samples. The

560   first effect of this absence is to make deprotonation of hydroxyl groups more difficult as, in

561   dioctahedral smectites, $MeFe^{3+}OH$ groups are known to deprotonate preferentially (Heller-

562 Kallai, 1975a, 2001; Russel, 1979; Jaymes and Bigham, 1987). The second effect is the

563 absence of cations that may be reduced in the octahedral sheet of trioctahedral smectites. The

564 combination of these two effects prevents building a strong layer charge deficit in the

565 octahedral sheet of trioctahedral smectites. The third factor leading to the lack of reactivity of

566 trioctahedral smectite is the obvious impossibility for cations to migrate in this octahedral

567 sheet which is fully occupied.

568 *Influence of structural Fe on smectite destabilization.* In the above conceptual model for

569 smectite destabilization, the effect of an increased proportion of structural iron on smectite

570 destabilization is dual. The first effect arises from the increased proportion of $MeFe^{3+}OH$

571 groups that will readily deprotonate when in contact with metal iron. The larger number of

572 deprotonated hydroxyl groups requires in turn the presence of a larger number of Fe^{2+} cations

573 in smectite interlayers to balance the charge. The second effect is directly related to the

574 increased proportion of structural Fe^{3+} in smectite octahedral sheet. This allows for a larger

575 proportion of smectite octahedral sheets to present dramatic charge deficit leading to the

576 migration of interlayer Fe^{2+} in the 2:1 layer, thus destabilizing it. On the other hand, the

577 presence of Fe^{3+} in smectite tetrahedral sheet does not enhance smectite reactivity as these

578 cations cannot be reduced because of steric constrains arising from their tetrahedral

579 environment.

580

581   CONCLUSION

582

583   The present study aimed at assessing the stability of smectites, which represent the

584 reactive components of engineered and geological barriers, when in contact with metal iron at

585 temperatures realistic in the context of nuclear waste disposal (80°C). Dioctahedral smectites

586 are thoroughly destabilized under such conditions, leading to the precipitation of magnetite

587 and of 1:1 iron-rich phyllosilicates [odinite, crondstedtite – Lantenois (2003), Lantenois *et al.*

588 (2005)]. Smectite destabilization is systematic for neutral-to-basic pH conditions (pH > 7),

589 whereas in mildly acidic to neutral pH conditions, a significant proportion of metal iron is

590 corroded to form magnetite without smectite destabilization.

591 An XRD method was developed to quantify the extent of smectite destabilization. This

592 method was validated against CEC measurements and IR spectroscopy results. Structural and

593 crystal-chemical factors favoring smectite destabilization were thus determined. These

594 parameters include the amount of octahedral iron, the presence of tetrahedral substitutions,

595 and the nature of interlayer cations, and a conceptual model was hypothesized to account for

596 smectite destabilization. According to this model, the formation of trioctahedral clusters

597 resulting from the migration of Fe^{2+} cations into the octahedral sheet of the 2:1 layer is

598 responsible for smectite destabilization as tetrahedral sheets are unable to accommodate the

599 larger dimensions of these domains.

600 In agreement with experimental results, the dioctahedral character of the initial

601 smectite is an essential condition for its destabilization in the proposed model. As a result the

602 non-reactivity of trioctahedral smectites appears as an important point for the conception of

603 engineered barriers for nuclear waste disposal, although natural deposits of trioctahedral

604 smectite are uncommon.

605

606 ACKNOWLEDGMENTS

607

615

616   **REFERENCES**

617

618   Aogaki, R. (1999) Non-equilibrium fluctuations in the corrosion. pp 217-305 in: Modern

619   aspects of electrochemistry (R.E White, B.E. Conway and J.O'M. Bockris editors).

620   Kluwer, New York.

621   Bailey, S.W. (1980) Structures of layer silicates. pp. 1-123 in Crystal Structures of Clay

622   Minerals and their X-ray Identification (G.W. Brindley and G. Brown editors).

623   Mineralogical Society, London.

624   Ben Brahim, J., Armagan, G., Besson, G. and Tchoubar, C. (1983a) X-ray diffraction studies

625   on the arrangement of water molecules in a smectite. I. Homogeneous two-water-layer

626   Na-beidellite. *Journal of Applied Crystallography*, **16**, 264-269.

627   Ben Brahim, J., Besson, G. and Tchoubar, C. (1983b) Layer succession and water molecules

628   arrangement in a homogeneous two-water layer Na-smectite. Pp. 65-75 in:

629   *Proceedings of the 5th Meeting of the European Clay Groups*, Prague.

630   Ben Brahim, J., Besson, G. and Tchoubar, C. (1984) Etude des profils des bandes de

631   diffraction X d'une beidellite-Na hydratée à deux couches d'eau. détermination du

632   mode d'empilement des feuillets et des sites occupés par l'eau. *Journal of Applied*

633   *Crystallography*, **17**, 179-188.

634   Besson, G. and Tchoubar, C. (1980) Exemple d'ordre-désordre par rotation des feuillets dans

635   la montmorillonite potassique. *Bulletin de Minéralogie,* **103**, 429-433.

636 Brindley, G.W. and Ertem G. (1971) Preparation and solvation properties of some variable

637   charge montmorillonites. *Clays and Clay Minerals*, **19**, 399-404.

638 Chang, F.R.C., Skipper, N.T. and Sposito, G. (1995) Computer simulation of interlayer

639   molecular structure in sodium montmorillonite hydrates. *Langmuir*, **11**, 2734-2741.

640 Cosultchi, A., Rossbach, P. and Hernandez-Calderon, I. (2003) XPS analysis of petroleum

641   well tubing adherence. *Surface and Interface Analysis*, **35**, 239-245.

642 Cuadros, J. and Altaner, S.P. (1998) Compositional and structural features of the octahedral

643   sheet in mixed-layer illite/smectite from bentonites. *European Journal of Mineralogy*,

644   **10**, 111-124.

645 Emmerich, K., Madsen, F. T. and Kahr G. (1999) Dehydroxylation behavior of heat-treated

646   and steam-treated homoionic *cis*-vacant montmorillonites. *Clays and Clay Minerals*,

647   **47**, 591-604.

648 Farmer, V.C. (1974) The IR Spectra of minerals. 539 p. Mineralogical Society, London.

649 Gaboriau, H. (1991) Interstratifiés smectite-kaolinite de l'Eure. Thesis, Université d'Orléans,

650   274p.

651 Gates, W.P., Slades, P.G., Manceau, A. and Lanson, B. (2002) Site occupancies by iron in

652   nontronites. *Clays and Clay Minerals*, **50**, 223-239.

653 Glaeser R. and Fripiat J. J. (1976) Hydratation des smectites et démixtion des cations Li, Na

654   en fonction de la localisation des substitutions isomorphiques. *Clay Minerals*, **11**, 93-

655   99.

656 Goodman, B.A., Russell, J.D., Fraser, A.R. and Woodhams, F.W.D. (1976) A mössbauer and

657   I.R. spectroscopic study of the structure of nontronite. *Clays and Clay Minerals*, **24**,

658   53-59.

659 Greene-Kelly, L. (1955) Dehydration of montmorillonite minerals. *Mineralogical Magazine*,

660   **30**, 604-615.

661 Guillaume, D., Neaman, A., Cathelineau, M., Mosser-Ruck, R., Peiffert, C., Abdelmoula, M.,

662   Dubessy, J., Villieras, F., Baronnet, A. and Michau, N. (2003) Experimental synthesis

663   of chlorite from smectite at 300°C in the presence of metallic Fe. *Clay Minerals*, **38**,

664   281-302.

665 Habert, B. (2000) Réactivité du fer dans les gels et les smectites. Thesis, Université Paris 6,

666   Paris, 227p.

667 Hamilton, D.L. and Henderson, C.M.B. (1968) The preparation of silicate compositions by a

668   gelling method. *Mineralogical Magazine*, **36**, 832-838.

669 Heller-Kallai, L. (1975a) Interaction of montmorillonite with alkali halides. S. W. Bailey (ed.)

670   proceding of international clay conference, Mexico, p. 361-375.

671 Heller-Kallai, L. (1975b) Montmorillonite-alkali halide interaction : a possible mechanism of

672   illitization. *Clays and Clay Mineral*, **23**, 462-467.

673 Heller-Kallai, L. (2001) Protonation-deprotonation of dioctahedral smectites. *Applied Clay*

674   *Science*, **20**, 27-38.

675 Heller-Kallai, L. and Rozenson, I. (1981) Nontronite after acid or alkali attack. *Chemical*

676   *Geology*, **32**, 95-102.

677 Heller-Kallai, L. and Mosser, C. (1995) Migration of Cu ions in Cu montmorillonite heated

678   with and without alkali halides. *Clays and Clay Minerals*, **43**, 738-743.

679 Hillier, S. (2000) Accurate quantitative analysis of clay and other minerals in sandstones by

680   XRD: comparison of a Rietveld and a reference intensity ratio (RIR) method and the

681   importance of sample preparation. *Clay Minerals*, **35**, 291-302.

682 Hofmann, V. and Klemen, R. (1950) Verlust der Austauschfähigkeit von lithiumionen aus

683   Bentonit durch Erhitzung. *Zeitschrift für Anorganische und Allgemeine Chemie*, **262**,

684   95-99.

685   Jaymes, W. F. and Bigham, J. M. (1987) Charge reduction , octahedral charge, and lithium

686   retention in heated, Li-saturated smectites. *Clays and Clay Minerals*, **35**, 440-448.

687   Kamei, G., Oda, C., Mitsui, S., Shibata, M., Shinozaki, T. (1999) Fe(II)-Na ion exchange at

688   interlayers of smectite : adsorption-desorption experiments and a natural analogue.

689   *Engineering Geology*, **54**, 15-20.

690   Kloprogge, J.T., Komarnene, S. and Amonette, J.E. (1999) Synthesis of smectite clay

691   minerals: a critical review. *Clays and Clay Minerals*, **47**, 529-554.

692   Kohler, E. (2001) Réactivité des mélanges synthétiques smectite/kaolinite et

693   smectite/aluminium gel en présence d'un excès de fer métal. DRT, Université d'Evry

694   val d'Essonne, Evry, 101p.

695   Lantenois, S. (2003). Réactivité fer métal/smectites en milieu hydraté à 80°C. Ph.D. thesis,

696   Université d'Orléans, Orléans, 188p

697   Lantenois, S., Lanson, B., van Aken, P. A., Jullien, M., Muller, F. and Plancon A. (2005)

698   Experimental study of metal iron - smectites interactions at low temperature :

699   characterisation of the newly-formed phases. Geochimica Et Cosmochimica Acta (in

700   preparation).

701   Madejova, J. and Komadel, P. (2001) Baseline studies of the clay minerals society source

702   clays: infrared methods. *Clays and Clay Minerals*, **49**, 410-432.

703   Madejova, J., Arvaiova, B. and Komadel, P. (1999) FTIR spectroscopic characterization of

704   thermally treated Cu^{2+}, Cd^{2+} and Li^+ montmorillonites. *Spectrochimica Acta Part A*,

705   **55**, 2467-2476.

706   Madejova, J., Bujdak, J., Gates, W. P. and Komadel, P. (1996) Preparation and infrared

707   spectroscopic characterization of reduced-charge montmorillonite with various Li

708   contents. *Clay Minerals*, **31**, 233-241.

709   Madejova, J., Bujdak, J., Petit, S. and Komadel, P. (2000a) Effects of chemical composition

710   and temperature of heating on the infrared spectra of Li-saturated dioctahedral

711   smectites. (I) Mid-infrared region. *Clay Minerals*, **35**, 739-751.

712   Madejova, J., Bujdak, J., Petit, S. and Komadel, P. (2000b) Effects of chemical composition

713   and temperature of heating on the infrared spectra of Li-saturated dioctahedral

714   smectites. (II) Near-infrared region. *Clay Minerals*, **35**, 753-761.

715   Mamy, J. (1968) Recherches sur l'hydratation de la montmorillonite: Propriétés diélectriques

716   et structure du film d'eau. Thesis, Université de Paris 6, Paris, 142p.

717   McBride, M.B. and Mortland M.M. (1974) Copper (II) interactions with montmorillonite:

718   Evidence from physical methods. *Soil Science Society of America Proceedings*, **38**,

719   408-415.

720   Monier, G., Robert, J.-L. (1986) Evolution of the miscibility gap between muscovite and

721   biotite solid solutions with increasing lithium content : an experimental study in the

722   system K_2O-Li_2O-MgO-FeO-Al_2O_3-SiO-H_2O-HF at 600°C, 2 kbar p_{H2O} : comparison

723   with natural lithium micas. *Mineralogical Magazine*, 50, 641-651.

724   Mosser, C., Michot, L. J., Villieras, F. and Romeo, M. (1997) Migration of cations in

725   copper(II)-exchanged montmorillonite and laponite upon heating. *Clays and Clay*

726   *Minerals*, **45**, 789-802.

727   Norrish, K. (1954) The swelling of montmorillonite. *Discussions of the Faraday Society*, **18**,

728   120-134.

729   Palkova, H., Madejova, J. and Righi, D. (2003) Acid dissolution of reduced-charge Li- and

730   Ni-montmorillonites. *Clays and Clay Minerals*, **51**, 133-142.

731   Pelletier, M., Michot, L.J., Humbert, B., Barres, O., D'espinose de la Callerie, J.B. and

732   Robert, J.L. (2003) Influence of layer charge on the hydroxyl stretching of

733 trioctahedral clay minerals: A vibrational study of synthetic Na- and K-saponites. *American Mineralogist*, **88**, 1801-1808.

735 Perronnet, M. (2001) Etude des interactions fer-argile en condition de stockage géologique
736   profond des déchets nucléaires HAVL. DEA, ENS Géologie, Nancy, 33p.

737 Perronnet, M. (2004) Etude des interactions fer-argile en condition de stockage géologique
738   profond des déchets nucléaires HAVL. Ph.D. thesis, ENS Géologie, Nancy, 233p.

739 Pons, C.H., Rousseaux, F. and Tchoubar, D. (1981) Utilisation du rayonnement synchrotron
740   en diffusion aux petits angles pour l'étude du gonflement des smectites: I Etude du
741   système eau-montmorillonite-Na en fonction de la température. *Clay Minerals*, **16**, 23-
742   42.

743 Roux, J. and Volfinger, M. (1996) Mesures précises à l'aide d'un détecteur courbe. *Journal de*
744   *Physique*, **IV**, 127-134.

745 Russell, J.D. (1979) An infrared spectroscopic study of the interaction of nontronite and
746   ferruginous montmorillonites with alkali metal hydroxides. *Clay Minerals*, **14**, 127-
747   137.

748 Russell, J. and Fraser, A. (1994) Infrared methods in Clay mineralogy: spectroscopic and
749   chemical determinative methods. M.J. Wilson, Ed. Chapman and Hall, London, p. 11-
750   67.

751 Shannon, R. D. (1976) Revised effective ionic radii and systematic studies of interatomic
752   distances in halides and chalcogenides. *Acta Crystallographica A*, **32**, 751-767.

753 Skipper, N.T., Chang, F.R.C. and Sposito, G. (1995) Monte Carlo simulation of interlayer
754   molecular structure in swelling clay minerals. 1. Methodology. *Clays & Clay*
755   *Minerals*, **43**, 285-293.

756 Suquet, H.B. (1978) Propriétés de gonflement et structure de la saponite. Comparaison avec la
757   vermiculite. Thesis, Université Pierre et Marie Curie, Paris, 175p.

758   Suquet, H., IIyama, J.T., Kodama, H. and Pezerat, H. (1977) Synthesis and swelling

759   properties of saponites with increasing layer charge. *Clays and Clay Minerals*, **25**,

760   231-242.

761   Suquet, H., Malard, C., Copin, E. and Pezerat, H. (1981) Variation du paramètre b et de la

762   distance basale d_{001} dans une série de saponites à charge croissante: I Etats hydratés.

763   *Clay Minerals*, **16**, 53-67.

764   Tomoe, Y., Shimizu, M. and Nagae, Y. (1999) Unusual corrosion of a drill pipe in newly

765   developed drilling mud during deep drilling. *Corrosion*, **55**, 706-713.

766   Tournassat C., Charlet L. & Greneche J.-M. Interactions of Fe^{2+}, Zn^{2+}, and H_4SiO_4 at

767   clay/water interfaces: Distinguishing sorption, coadsorption, and surface oxidation

768   phenomena. Geochimica and Cosmochimica Acta, submitted

769   Vantelon, D., Pelletier, M., Michot, L.J., Barres, O. and Thomas, F. (2001) Fe, Mg and Al

770   distribution in the octahedral sheet of montmorillonites. An infrared study in the OH-

771   bending region. *Clay Minerals*, **36**, 369-379.

772

774

775 **Figure 1.** XRD patterns obtained on unreacted and reacted smectite samples (upper and lower

776 patterns, respectively). Montmorillonite, beidellite, nontronite and saponite samples were

777 reacted for 45 days with metal iron at 80°C (see text for details) (a) Sample SWy-2 ,(b)

778 Sample SAz-1, (c) Sample SbId, (d) Sample CP4, (e) Sample Garfield, (f) Sample SapCa-2,

779 and (g) Sample SapFe08. Scale factor (x3) over the 20-35°2θ CoKα range. Patterns were

780 normalized by pairs to the integrated intensity of corundum (012) reflection (solid line, S).

781 The (001) reflection and the (02,11) band of the clay samples are labeled. Q indicates the

782 presence of quartz impurities in some samples (dashed lines). Dotted lines indicate the

783 reflections of newly-formed phases. These phases are labeled M, L, and P for magnetite

784 (Fe_3O_4), lepidocrocite (γ-FeOOH), and a newly formed 1:1 phyllosilicate, respectively.

785 **Figure 2**. Method for quantifying the relative proportion of destabilized smectite using IR

786 spectroscopy. (a) IR spectrum of sample SWy-2 (unreacted) before subtraction of the

787 baseline. Si-O indicates the Si-O vibrations in phyllosilicates whereas Al-Al-OH, Al-Fe-OH

788 and Al-Mg-OH refer to the OH bending mode of the respective hydroxyl groups. Q denotes

789 the two vibrations bands of quartz. (b) Decomposition assuming three Guassian-shaped

790 contributions of the OH bending zone after baseline subtraction (sample SWy-2 unreacted).

791 **Figure 3**. SEM micrographs of unreacted and reacted samples. Metal iron particles in

792 unreacted and reacted SWy-2 sample are shown on (a) and (b), respectively. (c) and (d)

793 Smectite particles in the reacted sample SWy-2. (e) Smectite particles in the initial sample

794 SWy-2. (f) Smectite particles in the reacted Garfield sample. (g) Smectite particles in the

795 initial sample SapCa-2. (h) Smectite particles in the reacted SapCa-2.

796 **Figure 4**. Relative proportion of destabilized smectite calculated by XRD and CEC methods

797 (a) and by XRD and infrared methods (b). Solid square: sample SapCa-2; solid triangle:

798   sample SAz-1; solid circle: sample SWy-2; solid diamond: Garfield sample; open diamond:

799   Drayton sample. The (1:1) line is shown as a solid line.

800   **Figure 5**. XRD patterns obtained for unreacted SbId sample (a) and for reacted SbId sample

801   (b-e). (b), (c), (d) and (e) correspond to 5, 15, 30 and 45 day experiments, respectively. Scale

802   factor (x3) over the 20-35°2θ CoKα range. Patterns were normalized as in Figure 1. Other

803   labels and patterns as in Figure 1.

804   **Figure 6**. Evolution of the relative proportion of destabilized smectite as a function of

805   reaction time. Symbols as in Figure 4. Open triangles: sample SbId.

806   **Figure 7**. XRD patterns obtained on unreacted and reacted beidellite samples (upper and

807   lower patterns, respectively). Patterns are ranked as a function of their structural Fe^{3+} content

808   (Table 1). Samples were reacted for 45 days with metal iron at 80°C without controlling the

809   initial pH. (a) Sample SbS-1, (b) Drayton sample, and (c) sample SWa-1. Scale factor (x3)

810   over the 20-35°2θ CoKα range. Patterns were normalized as in Figure 1. Other labels and

811   patterns as in Figure 1.

812   **Figure 8**. Relative proportion of destabilized smectite after reaction with metal iron as a

813   function of their content of structural Fe^{3+} (Table 1) Relative proportion of destabilized

814   smectite amounts was estimated using XRD on 45 day experiments.

815   **Figure 9**. XRD patterns recorded on sample SWy-2 reacted with metal iron after K-, Ca-, and

816   Na-saturation (b, c, and d, respectively). Unreacted Na-saturated sample corresponds to the

817   raw SWy-2 sample (a). Scale factor (x3) over the 20-35°2θ CoKα range. Patterns were

818   normalized as in Figure 1. Other labels and patterns as in Figure 1.

819   **Figure 10**. Transmission electron micrographs of smectite particles from sample CP4.

820   "rolled" and "flat" particles are labeled (1) and (2), respectively.

821   **Figure 11**. Conceptual model leading to the destabilization of dioctahedral smectites as a

822   result of their interaction with metal iron. (a) Deprotonation of $MeFe^{3+}OH$ groups. (b)

823   Oxidation of metal iron as a result of its interaction with released protons. (c) Sorption of Fe^{2+}

824   cations on the edges of smectite particles and reduction of structural Fe^{3+} cations. (d)

825   Migration of solution Fe^{2+} cations in smectite interlayers to compensate for the layer charge

826   deficit. Part of this migration results from a Fe^{2+}-for-Na^+ exchange. With time, interlayer Fe^{2+}

827   cations migrate to the di-trigonal cavity and further to the octahedral sheet to compensate

828   locally for the charge deficit. (e) Coexistence of di- and tri-octahedral domains in the

829   octahedral sheet of smectite leads to its destabilization.

830

Table 1: Chemical composition of the initial smectite materials (structural formulae calculated per $O_{10}(OH)_2$) and relative proportion of smectite destabilized after reaction with metal iron for 45 days.

Sample	Garfield[a]	SWa-1[a]	Drayton[b]	CP4[b]	Sbld[c]	SbS-1[c,d]	SWy-2[c]	SAz-1[c]	SapCa-2[c]	SapFe08[c,d]
Nature[e]	N	FS	B	B	B	B	M	M	S	S
Tetrahedral										
Si	3.51	3.70	3.69	3.60	3.71	3.66	3.95	4.00	3.58	3.62
Al	0.49	0.30	0.31	0.40	0.29	0.34	0.05	-	0.39	-
Fe^{3+}	-	-	-	-	-	-	-	-	0.03	0.38
charge	-0.49	-0.30	-0.31	-0.40	-0.29	-0.34	-0.05	-	-0.42	-0.38
Octahedral										
Al	0.11	0.55	1.11	1.70	1.80	2.00	1.56	1.37	-	-
Fe^{3+}	1.86	1.31	0.47	0.30	0.12	-	0.21	0.07	-	0.00
Mg	0.02	0.13	0.44	-	0.08	-	0.23	0.56	3.00	3.00
occupancy	1.99	1.99	2.02	2.00	2.00	2.00	2.00	2.00	3.00	3.00
charge	-0.05	-0.16	-0.38	0.00	-0.08	0.00	-0.23	-0.56	0.00	0.00
Interlayer										
Na	0.09	0.03	-	-	0.08	0.33	0.14	0.05	0.34	0.39
Ca	0.20	0.20	0.17	0.15	0.10	-	0.05	0.24	0.05	-
Mg	-	-	0.18	-	-	-	-	-	-	-
K	0.04	0.05	-	0.09	0.08	-	0.01	0.01	0.02	-
charge	0.53	0.48	0.70	0.39	0.36	0.33	0.25	0.54	0.46	0.39
Smectite destab. (wt %)	95	90	70	40	60	0	50	20	0	0

Note: [a] From Gates *et al.* (2002). Interlayer composition of raw materials was determined from electron microprobe analysis, [b] EDX analysis on a transmission electron microscope, [c] electron microprobe analysis, [d] synthetic clays. [e] N, FS, B, M, S correspond to nontronite, ferruginous smectite, beidellite, montmorillonite and saponite respectively.

Table 2: Chemical composition of the solution after reaction of smectite samples with metal iron for 45 days.

	Si	Al	Fe	Mg	Na	Ca	K	Initial pH	Final pH
SapCa-2	0.0	0.0	0.0	0.0	10.0	4.0	0.0	9.5	10.0
SapCa-2 Ref	0.0	0.0	0.0	0.0	7.0	2.0	0.0	9.5	9.5
SWy-2	6.5	0.1	0.0	0.3	115	3.5	3.0	10.0	10.5
SWy-2 Ref	0.0	0.0	0.0	0.0	11.0	0.0	0.0	10.0	10.0
Sbld	2.0	0.4	0.0	0.3	17.0	28.0	14.0	7.5	7.5
Sbld Ref	0.0	0.0	0.0	0.0	1.0	2.0	1.0	7.5	7.5
Garfield	0.0	0.0	0.0	0.0	17.5	22.5	1.0	8.5	9.5
Garfield Ref	0.0	0.0	0.0	0.0	10.0	1.0	2.0	8.5	9.0

Note: Concentrations are given in $mg.L^{-1}$. Initial and final pH values were measured before and after reaction, respectively. Regular sample names correspond to the reaction of a given smectite sample with metal iron for 45 days at 80°C. Ref samples correspond to the reaction of a given smectite sample for 45 days at 80°C without metal iron.

Table3: Relative proportion of smectite destabilized (weight %) as a function of the initial solution pH.

pH	SWy-2	SapCa-2	Garfield
6	0%	0%	0%
8	50%	-	95%
10	50%	0%	-
12	50%	-	-

Note: Relative proportion of destabilized smectite is estimated using the XRD method.

Table 4: Relative proportion of smectite destabilized (weight %) as a function of the cation interlayer composition.

	SAz-1	SWy-2	Garfield
K	-	0%	50%
Ca	20%*	20%	95%*
Na	40%	50%*	-

Note: Relative proportion of destabilized smectite is estimated using the XRD method. * indicate raw samples, with the corresponding predominant interlayer cation.

Figure 1 :

Figure 2 :

Figure 3 :

a

2 µm

b

2 µm

c

3 µm

d

2 µm

e

2 µm

f

2 µm

g

3 µm

h

4 µm
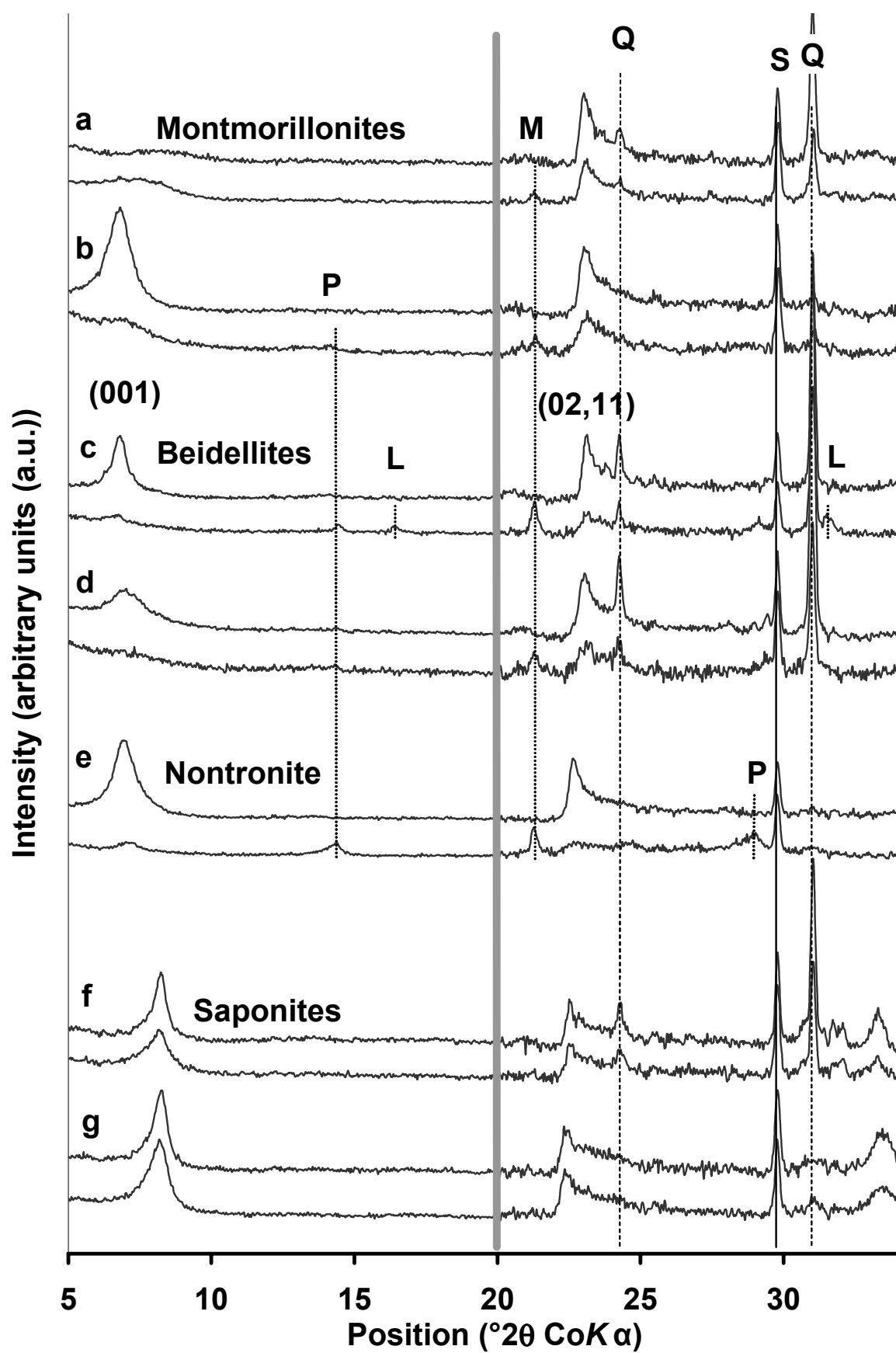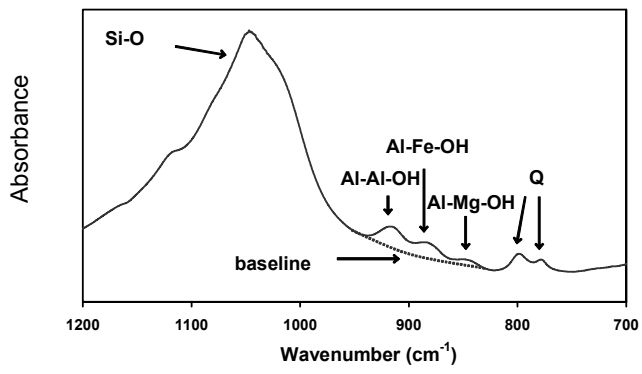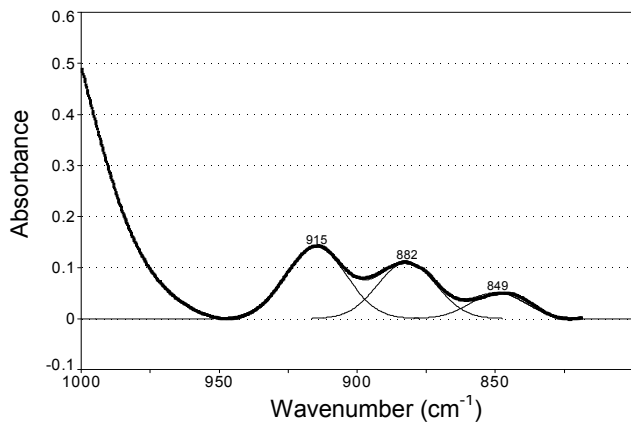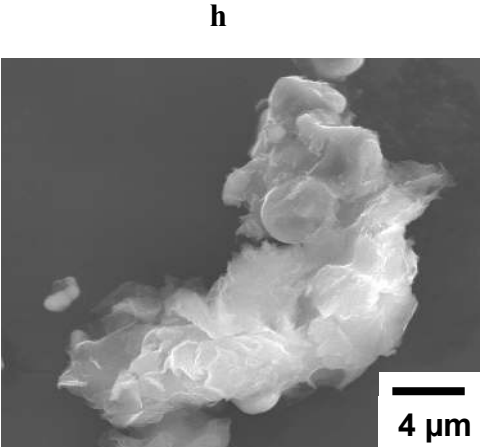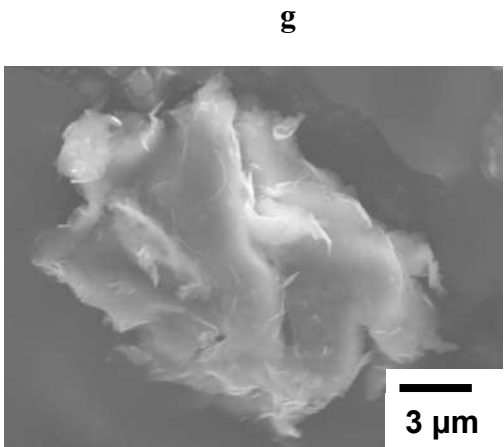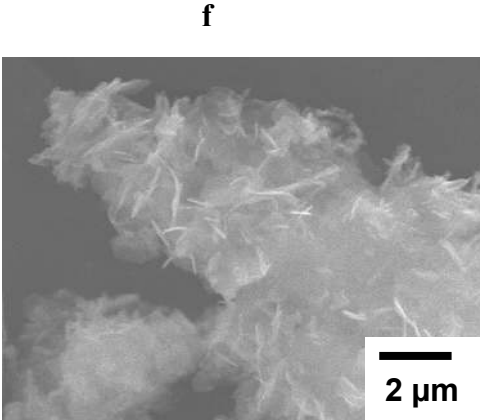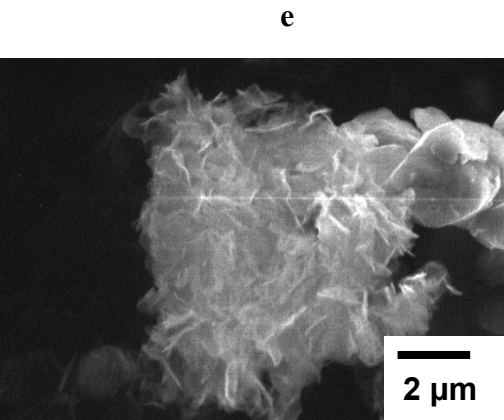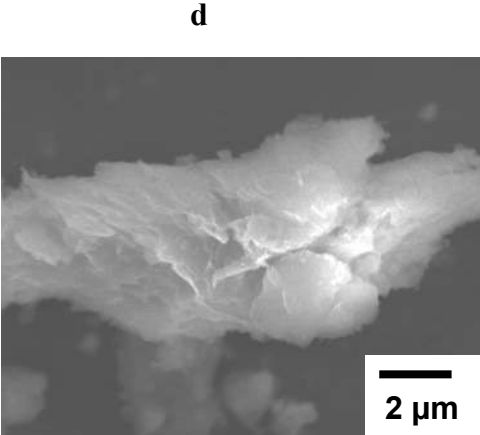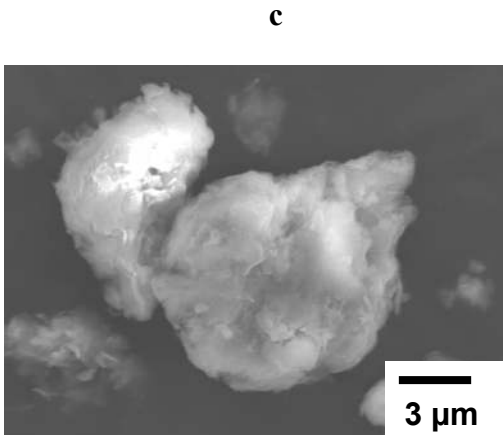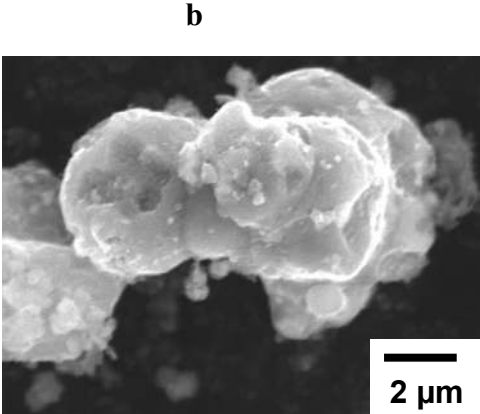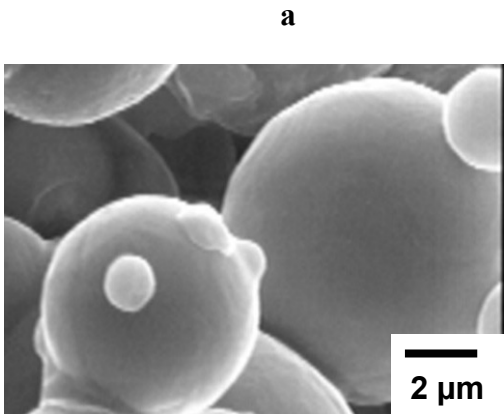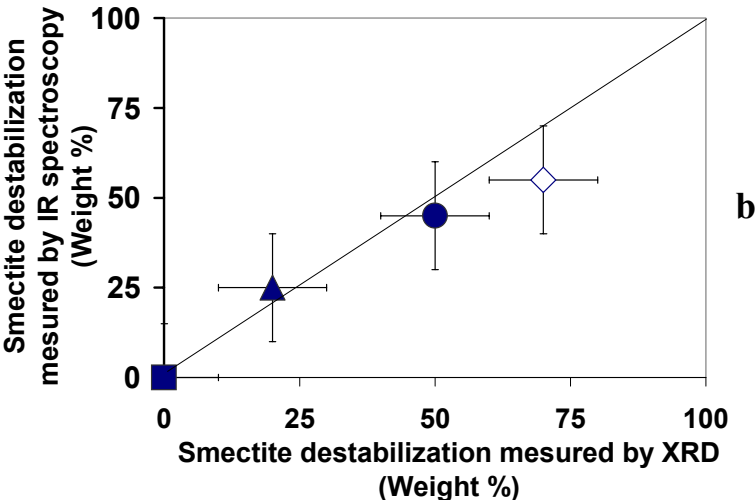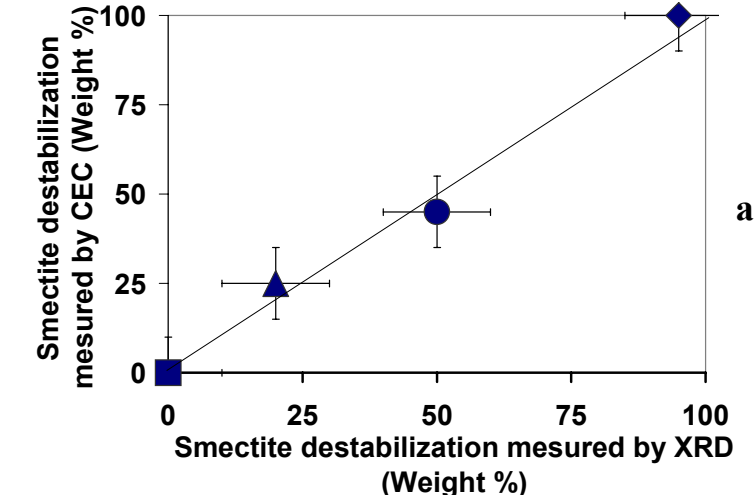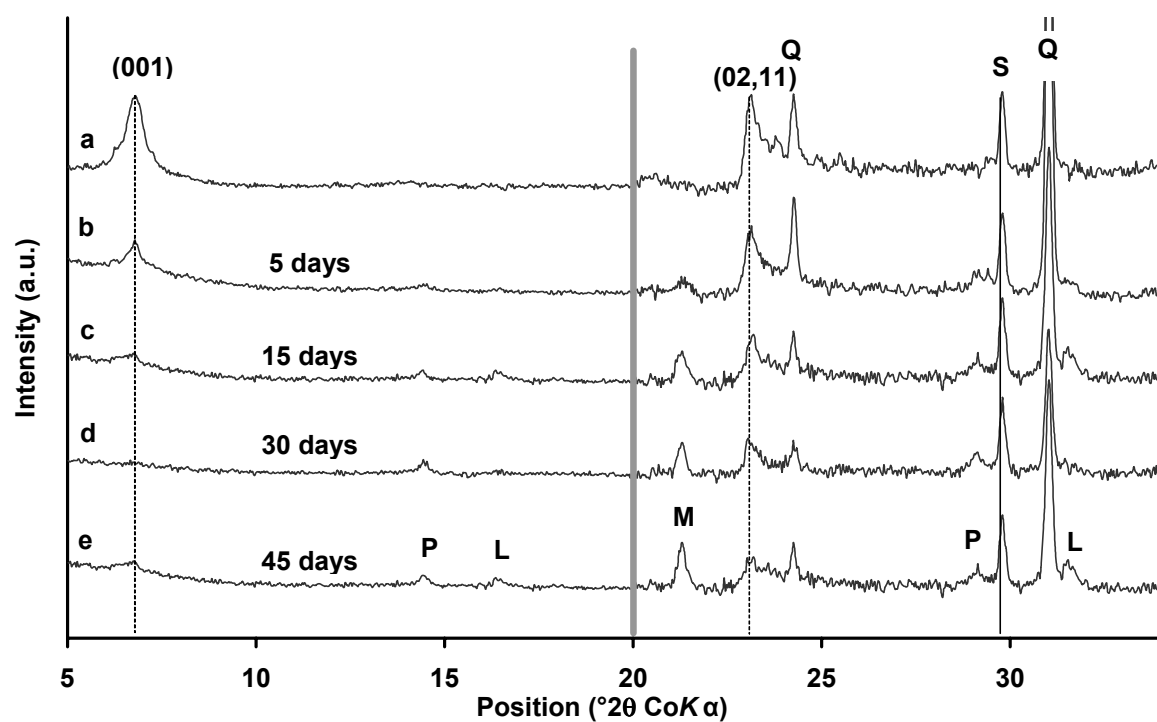
Figure 4 :

Figure 5 :

Figure 6 :
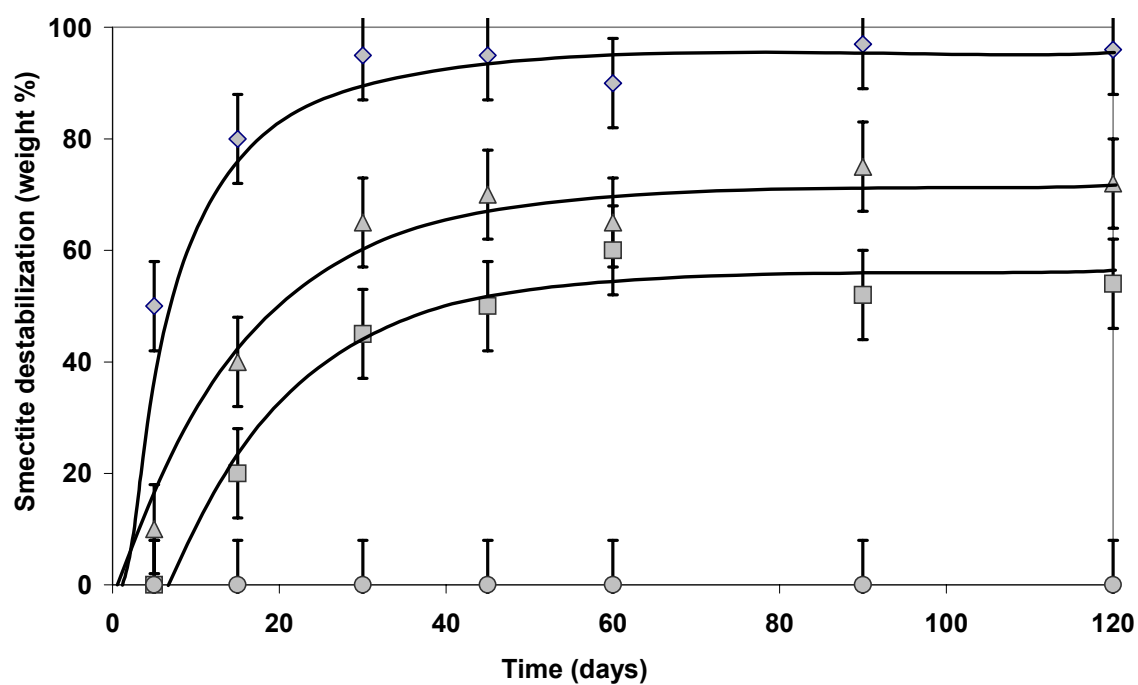
Figure 7 :
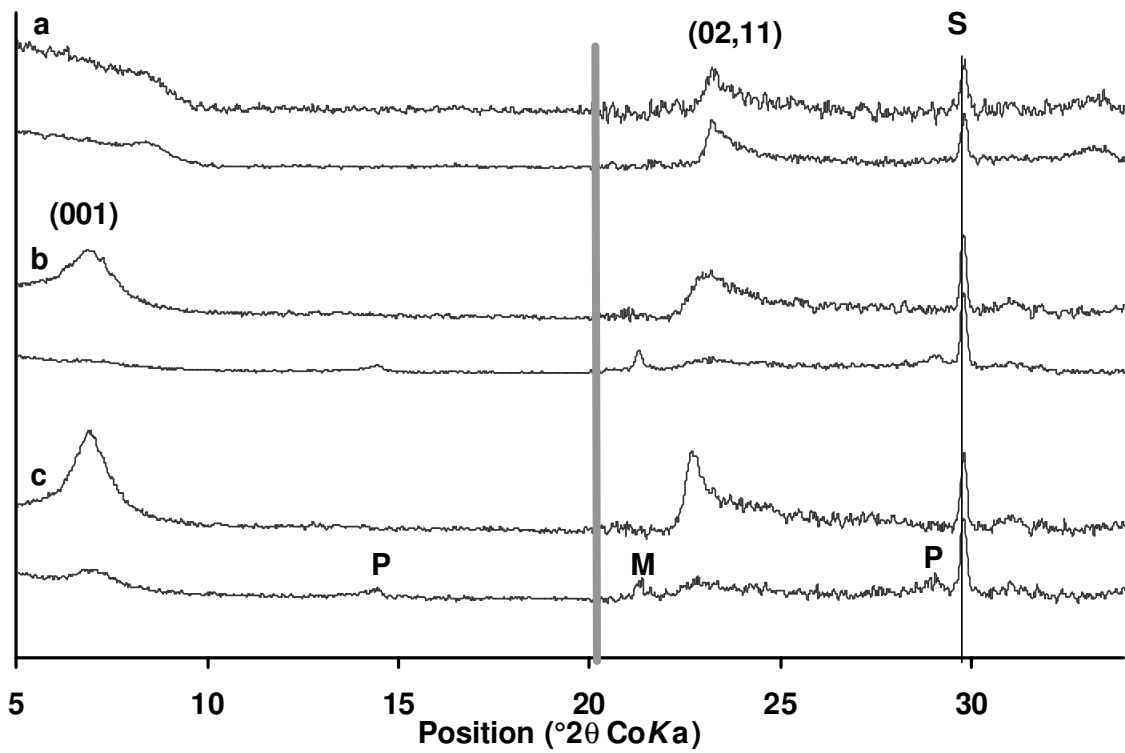
Figure 8 :
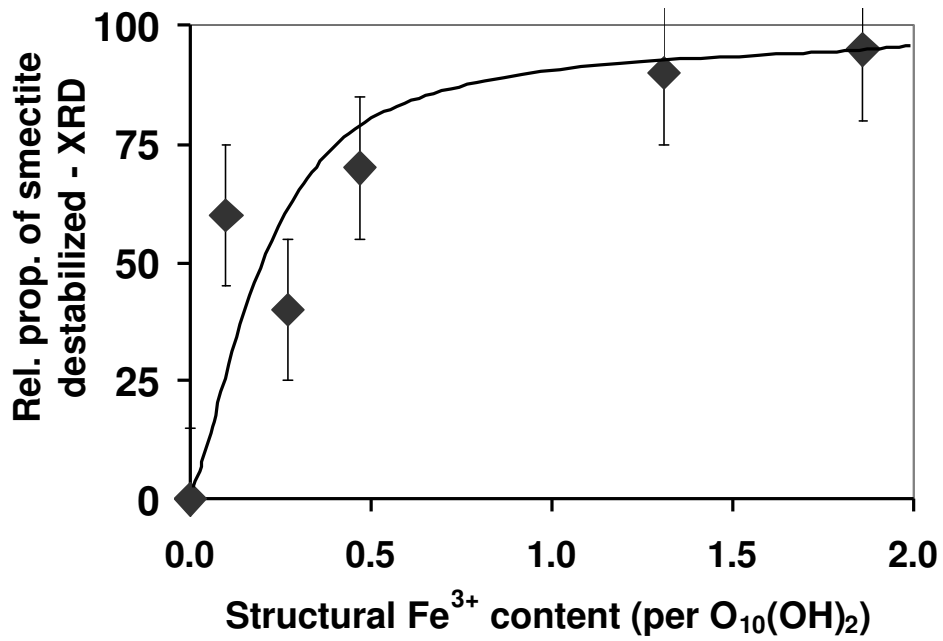
Figure 9 :

Figure 10 :

Figure 11